

1–5 μm imaging of 3CRR galaxies: The K – z relation and the geometry of the torus

Chris Simpson,¹ Martin Ward,² and J. V. Wall³

¹*Subaru Telescope, National Astronomical Observatory of Japan, 650 N. A‘ohōkū Place, Hilo, HI 96720, U.S.A.*

²*X-ray Astronomy Group, Department of Physics and Astronomy, University of Leicester, Leicester LE1 7RH*

³*Astrophysics, Department of Physics, University of Oxford, Oxford OX1 3RH*

27 October 2018

ABSTRACT

It has been claimed by Taylor et al. that the low-redshift end of the K – z relation for radio galaxies is too bright by about half a magnitude due to contributions from the obscured quasar nuclei. Such a result has major implications for the use of the K -band Hubble diagram in understanding the cosmological evolution of radio galaxies. In this paper we present 1–5 μm imaging data of a nearly-complete sample of low-redshift radio galaxies; this approach allows us to accurately determine the strengths of any unresolved nuclear components in the galaxies. We detect nuclear sources in five targets, whose broad-band colours are consistent with reddened quasar spectra. In all five cases the ratio of the inferred intrinsic near-infrared luminosity to the narrow-line luminosity is typical of quasars. We find a correlation between the inferred nuclear extinction and core-to-lobe ratio, which places constraints on the geometry of the torus. We find evidence for a shift of the K – z relation to fainter magnitudes, but by a much smaller amount (~ 0.1 mag) than Taylor et al. determined. Under the assumption that the nuclear sources in radio galaxies have the same intrinsic near-infrared spectra as quasars, our multi-wavelength images allow us to limit any possible shift to less than 0.3 magnitudes.

Key words: galaxies: active – galaxies: nuclei – galaxies: photometry – infrared: galaxies – radio continuum: galaxies

1 INTRODUCTION

It has been proposed that powerful FR II (see Fanaroff & Riley 1974) radio galaxies and radio loud quasars are intrinsically the same objects, with all observed differences being a result of the angle between the line of sight and the radio axis (Scheuer 1987; Barthel 1989). While objects classified as “narrow-line radio galaxies” do not display obvious broad lines in their optical spectra, broad lines have been seen either in the near-infrared (e.g. Hill, Goodrich & DePoy 1996) or in polarized light (e.g. Young et al. 1996). In addition, the detection of unresolved nuclei in near-infrared observations of radio galaxies (e.g. Djorgovski et al. 1991; Simpson, Ward & Wilson 1995), where the optical depth is lower, indicates the presence of a quasar-like nucleus in the centres of these objects. Since quasars can outshine their host galaxies by factors ranging from a few (e.g. Dunlop et al. 1993; Taylor et al. 1996, hereafter T96) to more than 100 in extreme cases (e.g. PDS 456; Simpson et al. 1999), even if only a few per cent of the nuclear light is transmitted it can still make a major contribution to the integrated luminosity.

It has long been known that the brightest radio galaxies,

i.e. those in the 3CRR catalogue of Laing, Riley & Longair (1983), are brighter in the near-infrared by about a magnitude at $z \approx 1$ than they are at low redshift. This amount of dimming as cosmic time increases is consistent with passive evolution of their stellar populations (Lilly & Longair 1984; Lilly, Longair & Allington-Smith 1985b). While some 3C radio galaxies at $z \approx 1$ suffer significant contamination from non-stellar radiation (Rawlings et al. 1995; Simpson, Rawlings & Lacy 1999), this does not have a significant impact on the locus of the K – z relation. However, radio galaxies from the fainter 6C and B2 radio surveys are 0.6 mag fainter at K than the 3C objects at these redshifts (Eales et al. 1997), whereas there is no correlation between radio and host galaxy luminosities locally. Furthermore, the 6C/B2 galaxies lie *below* the no-evolution curve.

The possibility that there is significant non-stellar contamination at *low* redshift is one that therefore needs to be investigated. A study by T96 claimed that the true locus of the K – z relation at low redshift may be half a magnitude fainter than previously thought due to contamination from the non-stellar nucleus. In this paper, we perform a similar analysis to that of T96 on an unbiased sample of radio galax-

ies from the catalogue of Laing et al. (1983). In Section 2 we describe our sample selection and observational technique. In Section 3 we briefly describe the two-dimensional fitting procedure used to separate the nuclear and host galaxy properties in our J and K images, and present the results of this analysis, together with aperture photometry of the longer-wavelength images. In Section 4 we use these results to examine the nature of the stellar and non-stellar components of radio galaxies, and infer the intrinsic luminosities of the nuclear sources and the line of sight obscurations towards them. In Section 5 we attempt to infer the geometry of this obscuring material, and in Section 6 we discuss the implications of our analysis on the low-redshift end of the K - z relation and compare our results with those of T96. Finally, we summarize our results in Section 7. Throughout this paper we adopt $H_0 = 50 \text{ km s}^{-1} \text{ Mpc}^{-1}$, $q_0 = 0.5$, and $\Lambda = 0$. Our convention for spectral index, α , is such that the flux density at a frequency ν , $S_\nu \propto \nu^{-\alpha}$.

2 SAMPLE SELECTION AND OBSERVATIONS

We selected our targets from the 3CRR catalogue of Laing et al. (1983). This catalogue is essentially complete and, by virtue of being selected at low frequency, does not preferentially include sources observed close to the radio axis whose fluxes are enhanced by Doppler boosted cores. It is therefore an unbiased sample of radio galaxies, except in the sense that it consists of the most radio-luminous objects. We excluded objects with known broad $H\alpha$, as determined by the high-quality spectrophotometric observations of Laing et al. (1994, hereafter L94); we did not however exclude 3C 234 since the broad $H\alpha$ seen is believed to be entirely scattered (Antonucci 1984; Young et al. 1998). This criterion supplied an upper redshift cutoff of $z < 0.43$, in order that $H\alpha$ still be present in the optical spectra. From those objects visible from the 3.8-m United Kingdom Infrared Telescope (UKIRT) in early January, we selected only those galaxies with strong optical emission lines (Class A; Hine & Longair 1979). The reasons for this were twofold. First, the low-ionization (“optically dull”, Class B) radio galaxies may not be part of the quasar–radio galaxy unification paradigm – they are predominantly low-power objects with an FRI radio morphology. Secondly, since emission-line luminosity is a good indicator of the power of the active nucleus (Rawlings & Saunders 1991), it follows that these objects will have less luminous nuclei in the near-infrared and are therefore likely to be below our detection threshold. We were able to observe ten of the eleven objects thus selected, with 3C 123 being excluded from our programme solely because it was never at a suitable hour angle when the time came to choose the next target. We present details of the sample in Table 1, including observed 178 MHz and [O III] $\lambda 5007$ fluxes and rest frame luminosities. Although the data of L94 is of a consistently high quality, their choice of a narrow slit necessarily meant a loss of extended emission line flux. This effect is especially pronounced in the closest radio galaxies, where the line emission can be extended over many arcseconds (see, e.g., Baum et al. 1988). We have therefore chosen not to use fluxes from L94’s data in those cases where a larger aperture measurement is available that contains a significantly larger flux. We were unable to locate large aperture measurements

for 3C 42 or 3C 153, although these are the two most distant objects in our sample and we can expect the spectroscopic slit of L94 to include virtually all the line emission.

All the images presented here were obtained on UKIRT in photometric conditions, using IRCAM3 with a nominal scale of $0.286 \text{ arcsec pixel}^{-1}$. Most observations were made on the nights of UT 1996 Jan 3–6, although 3C 33, 3C 153, and 3C 171 were observed during an earlier run on UT 1995 Jan 3–5 as part of a pilot study. Each target was observed through the $JKL'M$ filters, with typical on-source exposure times of 18 minutes at J and K and 30 minutes at L' and M . Most of the radio galaxies are sufficiently compact at J and K compared to the size of the array that it was possible to use standard jittering techniques and therefore there was no need for “off-source” observations to produce a flatfield image. In these cases, each observation consisted of taking two sets of nine jittered frames of 60 s duration each (split into shorter, background-limited exposures). For those objects with $z < 0.1$, however, nearby regions of sky were used to enable flatfielding and sky subtraction. The much higher background in the thermal-infrared (L' and M) meant that only the central regions of the radio galaxies were detected with any significance, and even the closest objects could be jittered about the array. However, to permit accurate flatfielding given the rapid background variations, shorter exposure times were necessary and each observation was split into sets of five frames of 30 s (L') or 15 s (M), each of which was again comprised of a number of shorter, background-limited exposures. Due to time constraints, we were unable to observe two of our targets (3C 42 and 3C 84) at M .

Data reduction was performed in the following manner. Each observation was split into its sets of nine (at J and K) or five (at L' and M) separate exposures, and these were dealt with as separate entities. First, an appropriate dark frame was subtracted from all the images. Then a flat field was produced by median-filtering either the sky frames (if the source was at $z < 0.1$) or the object frames (for cases where no off-source observations were made), after scaling each frame to have the same median pixel value. Each object frame was then divided by a normalized version of this flatfield, and these images were registered, using stars and galaxies visible on the individual images where possible, or the nominal telescope offsets otherwise. An iterative technique was used to determine the DC offsets between regions of overlap in separate frames, and the images were averaged. At this stage, the separate sets were averaged together to produce the final image. The seeing was measured from stars in the individual exposures to be in the range 1.0–1.2 arcsec FWHM (about 4 pixels) and the registration uncertainties did not cause the FWHM of stars in the final coadded images to increase by a measurable amount.

Images of photometric standard stars were taken throughout the course of each night. One standard star was imaged five times in each filter for each radio galaxy. Multiple coadds were used both to improve the signal-to-noise ratio, and to ensure that each observation had a similar exposure time to the individual radio galaxy observations. In this way, the point spread function (PSF) of the standard star would sample the same longer-term seeing variations as the galaxy images. Flux calibration solutions were determined separately for each night of observation, with the r.m.s. dispersion for each night typically being 4% at J and

Table 1. The sample of radio galaxies studied. Radio fluxes and spectral indices are from Laing et al. (1983), although the radio fluxes have been multiplied by 1.09 to put them on the scale of Baars et al. (1977). The Galactic extinctions used to deredden the [O III] luminosities are from NED. References for [O III] flux: YO = Yee & Oke (1978), assuming $\lambda_{5007}/\lambda_{4959} = 3$; L = L94 and Laing et al. (2000).

Name	IAU name	z	$S_{178\text{ MHz}}$ (Jy)	α	$\log L_{178\text{ MHz}}$ (W Hz^{-1})	f_{5007} (10^{-18} W m^{-2})	$\log L_{5007}$ (W) observed	$\log L_{5007}$ (W) dereddened	[O III] ref	$E(B - V)$
3C 33	0106+130	0.0595	59.3	0.76	26.95	108	35.20	35.23	YO	0.02
3C 42	0125+288	0.3950	13.1	0.73	27.91	1.6	34.96	35.01	L	0.05
3C 79	0307+169	0.2559	33.2	0.92	27.93	48.5	36.08	36.19	L	0.10
3C 84	0316+413	0.0172	66.8	0.78	25.93	544	34.84	35.07	L	0.17
3C 98	0356+102	0.0306	51.4	0.78	26.32	76	34.48	34.65	YO	0.13
3C 153	0605+480	0.2769	16.7	0.66	27.73	2.2	34.80	35.04	L	0.23
3C 171	0651+542	0.2384	21.3	0.87	27.68	21.7	35.68	35.74	L	0.06
3C 192	0802+243	0.0598	23.0	0.79	26.54	57	34.94	34.98	YO	0.03
3C 223	0936+361	0.1368	16.0	0.74	27.10	43.8	35.53	35.53	L	0.00
3C 234	0958+290	0.1848	34.2	0.86	27.68	208	36.45	36.47	YO	0.01

Table 2. Photometry in a 3-arcsec aperture. Limits are 3σ .

Galaxy	J	K	L'	M
3C 33	14.41 ± 0.04	13.16 ± 0.04	11.89 ± 0.08	11.17 ± 0.13
3C 42	17.52 ± 0.02	16.06 ± 0.03	> 15.08	not observed
3C 79	16.37 ± 0.03	14.79 ± 0.06	12.96 ± 0.08	> 12.43
3C 84	13.41 ± 0.03	11.90 ± 0.05	9.66 ± 0.06	not observed
3C 98	13.83 ± 0.02	12.60 ± 0.03	12.19 ± 0.07	> 12.36
3C 153	16.71 ± 0.04	15.25 ± 0.04	> 14.97	> 12.71
3C 171	16.97 ± 0.04	15.71 ± 0.04	> 15.23	> 12.44
3C 192	14.43 ± 0.03	13.46 ± 0.05	13.39 ± 0.08	> 12.28
3C 223	16.02 ± 0.04	14.58 ± 0.05	12.91 ± 0.07	11.79 ± 0.20
3C 234	15.33 ± 0.03	13.08 ± 0.05	10.50 ± 0.06	9.91 ± 0.08

K and 7% at L' and M . Aperture photometry from our images agrees with that of Lilly & Longair (1984) and Lilly, Longair & Miller (1985a) to within the quoted uncertainties. In Table 2 we list the photometry measured in a 3-arcsec aperture, which is more appropriate for detecting red nuclear sources.

3 SEPARATION OF NUCLEUS AND HOST GALAXY

Thermal emission from the telescope is very strong longward of $2.5\mu\text{m}$, resulting in a vastly increased background and a large drop in sensitivity. In addition, the strength of the quasar nucleus relative to the host galaxy increases with wavelength due to its red colour. We therefore undertake different analyses for the short (JK) and long ($L'M$) wavelength data.

In our J and K images, the host galaxies are well-detected out to large radii and are likely to dominate over the nuclei, even in fairly small apertures. Methods which attempt to estimate the flux of a nuclear source by using aperture photometry to correct small aperture measurements for starlight are prone to overestimate the strength of the source (Simpson 1994b) and it is necessary to model the galaxy in order to obtain a reliable measurement. At longer wavelengths, the host galaxy is not detected with great signif-

icance due to the bright thermal background, and simpler methods can be employed.

3.1 Two-dimensional modelling

To enable the most direct comparison possible of our results with those of T96, we have used an almost identical analysis technique on our data. We refer the reader to that paper for a more detailed description of the method, and for a discussion of its advantages over the more common (and simpler) one-dimensional analysis (e.g. Simpson et al. 1995).

The two-dimensional approach involves constructing a model image derived from fitting parameters and comparing this with the actual data, using an error frame to allow a quantitative χ^2 minimization. The assumed model was an elliptical galaxy obeying a de Vaucouleurs law (de Vaucouleurs 1948) and an unresolved nuclear source. There are five parameters used to construct the model:

- (i) The luminosity of the nuclear source, L_{nuc}
- (ii) The luminosity of the host galaxy, L_{host}
- (iii) The effective (half-light) radius of the host galaxy, r_e
- (iv) The position angle of the major axis of the host galaxy, Θ
- (v) The axial ratio of the host galaxy, a/b

The pixel location of the centre of the galaxy, (x_c, y_c) , was determined using iterative centroiding, and construction of the model galaxy proceeded as follows. Each pixel in the

image was divided into 400 subpixels, and the flux in each of these subpixels was computed based on the parameters of the galaxy model. This amount of subpixelation ensures that the flux in the central pixel is never underestimated by more than 0.14%, and any overestimation of the nuclear source flux as a result will be negligible. The nuclear source was then added by increasing the value of the central pixel (x_c, y_c) by the appropriate amount. This nucleus-plus-galaxy model was convolved with the adopted PSF to produce a simulated image.

The quality of fit for the simulated image was determined by the χ^2 statistic,

$$\chi^2 = \sum \left(\frac{z(x, y) - \zeta(x, y)}{\sigma(x, y)} \right)^2,$$

where $z(x, y)$ and $\zeta(x, y)$ are the values of the (x, y) pixel in the real data and the simulated image respectively, and $\sigma(x, y)$ is the uncertainty assigned to this pixel. We constructed an error frame in exactly the same manner as T96, although the sampling errors are smaller for our data due to the smaller pixel scale. This procedure results in good error estimation, and the images of the weighted residuals from the best-fit models appeared structureless. Companion objects and foreground stars were effectively excluded from the fitting procedure at this point by setting the pixel values of the error frame to some very large value in regions where a contaminating source was visible, thus giving such pixels a negligibly small weight in determining the quality of fit.

In virtually all cases, the radio galaxy occupied only a fraction of the total frame. To speed up the computational process, we therefore used only a subregion of the image for our analysis. We selected a square region which just encompassed the isophote whose intensity was 0.01% of the sky brightness, the level at which flatfielding uncertainties are expected to become important. Typically such a region was about 30 arcsec on a side. The exception was 3C 84, whose proximity meant that such an isophote was larger than the entire IRCAM3 field of view, and so we used the full array. We deviate from the method of T96 in the optimization algorithm we use. Instead of the Polak-Ribiere minimization of T96, we used a simulated annealing algorithm (Press et al. 1996). We first tested the fitting procedure on simulated galaxies to which noise had been added. After confirming that it successfully recovered the input parameters of the model, the fitting procedure was performed ten times in J and K for each radio galaxy, with two different starting simplexes for each of the five different PSFs. The results of the fit which produced the lowest value of χ^2 were used in later analysis.

We estimate the uncertainties in our fitting parameters by considering the variations in the results from the ten separate fits. However, not all PSFs were able to produce good fits, by which we mean a value of χ^2 close to that of the best fit, and we rejected those which did not. As expected, only the nuclear luminosity depends strongly on the PSF. Typically (for galaxies with $a/b \gtrsim 1.1$), the position angle is determined to 5° or better, while the uncertainty is as large as 10° for 3C 192 (with $a/b \approx 1.03$, the roundest galaxy in our sample). The axial ratio is always determined to better than 5%. Although the host galaxy luminosity is generally determined to $\sim 5\%$ r.m.s., the uncertainty in the effective radius is larger, ($\sim 10\%$), and the peak surface brightness

Table 3. Results of the fits to the J and K images. Listed are the nuclear and host galaxy (integrated out to infinite radius) magnitudes, their ratio in a 12-arcsec aperture, and the effective radius (in kpc), axial ratio and position angle of the host galaxy.

Galaxy		m_{nuc}	m_{host}	$\frac{L_{\text{nuc}}}{L_{\text{host}}}$ (12'')	r_e	a/b	Θ	χ^2_ν
3C 33	J	> 18.2	12.6	< 0.01	7.5	1.10	153	1.78
	K	16.6	11.7	0.02	5.9	1.09	158	2.05
3C 42	J	> 19.0	16.4	< 0.13	15.1	2.32	160	1.58
	K	> 18.1	14.9	< 0.07	12.9	1.95	162	1.01
3C 79	J	17.4	15.5	0.23	10.4	1.15	15	1.90
	K	15.6	14.2	0.35	8.0	1.07	11	1.27
3C 84	J	15.7	8.9	0.02	24.6	1.24	112	5.53
	K	12.6	7.9	0.15	25.2	1.26	114	8.25
3C 98	J	> 18.5	11.9	< 0.01	4.2	1.17	60	2.72
	K	> 17.2	10.8	< 0.01	4.5	1.16	62	1.27
3C 153	J	> 18.4	15.4	< 0.10	21.5	1.45	86	0.14
	K	> 17.5	14.0	< 0.07	21.5	1.37	87	0.22
3C 171	J	> 18.8	15.9	< 0.08	7.0	1.21	170	1.24
	K	> 17.8	14.5	< 0.06	8.6	1.33	156	1.88
3C 192	J	> 18.4	13.0	< 0.01	7.8	1.03	94	1.83
	K	> 17.4	12.1	< 0.01	7.7	1.04	101	1.65
3C 223	J	17.5	14.5	0.10	11.1	1.33	57	0.68
	K	14.9	13.6	0.50	13.7	1.42	59	1.32
3C 234	J	15.5	15.4	1.30	13.7	1.04	61	1.87
	K	13.6	13.8	1.66	12.2	1.21	81	1.17

can be uncertain by as much as $\sim 20\%$ (with there being a strong anti-correlation between effective radius and peak surface brightness). The fits we performed in the J and K filters for each galaxy were completely independent. However, it is expected that some quantities, such as the axial ratio and the position angle of the major axis, should be very similar in the two bands. The difference between the values of these quantities derived for each filter can therefore also be taken as a measure of the uncertainty.

For galaxies with large nuclear-to-host ratios (e.g. 3C 234) or large angular effective radii (e.g. 3C 84), the magnitude of the nuclear source was well-determined. However, for other sources it was quite sensitive to the PSF used, and in many cases, the best-fit nuclear flux was very faint and it became necessary to estimate some limit, fainter than which a source would not be considered a true detection. We estimate the uncertainty on the nuclear flux (in units of detector counts) to be $\sigma = \bar{e}\sqrt{n}$, where \bar{e} is the mean value of the error image in a 3-arcsec aperture and n is the number of pixels in this aperture. When the flux of the nuclear source is less than 5σ , we quote an upper limit. These limits vary slightly from source to source, depending on such things as the seeing, but are typically $J \approx 18.5$ and $K \approx 17.5$, or a few per cent of the integrated host galaxy luminosity. The size of the variations in the best fit value of the nuclear flux for different PSFs and starting simplexes was broadly consistent with this level of uncertainty. Contour plots of the data and our models can be found in Figs 1–10. The properties of the best-fitting models are listed in Table 3.

We make a comment regarding the K -band fit for 3C 98 listed in Table 3. This fit has $\chi^2/\nu = 25226/19876$, but the other nine fits all have $\chi^2 < 26000$ yet have nuclear sources as bright as $K = 14.9$. This is in marked contrast to the other model galaxies, where large variations in the best-fitting nuclear flux compared to the value in Table 3 were accompanied by large increases in χ^2 , and were presumably

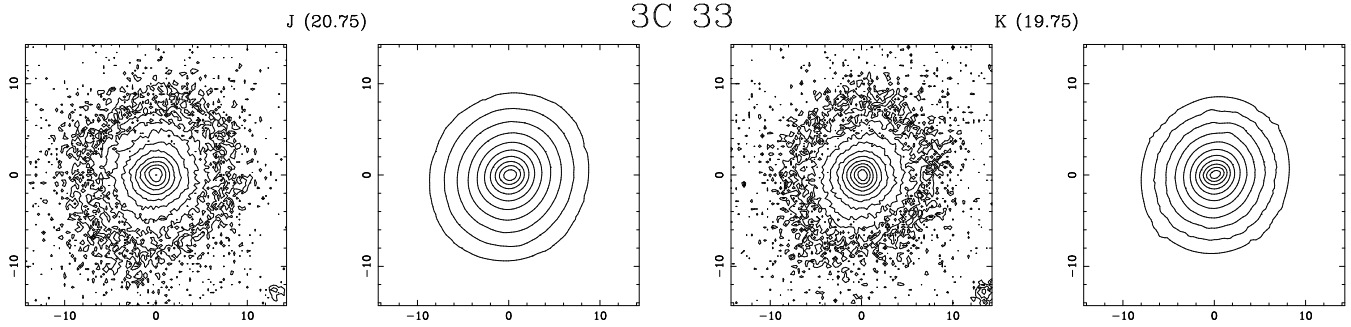


Figure 1. Images of 3C 33 and the best-fitting model at *J* (left two panels) and *K* (right two panels). The number in parenthesis indicates the value of the lowest contour plotted (in mag arcsec^{-2}), with successive contours spaced at 0.5 mag intervals. North is up and east is to the left. The axes are labelled in arcseconds. These images have not been smoothed.

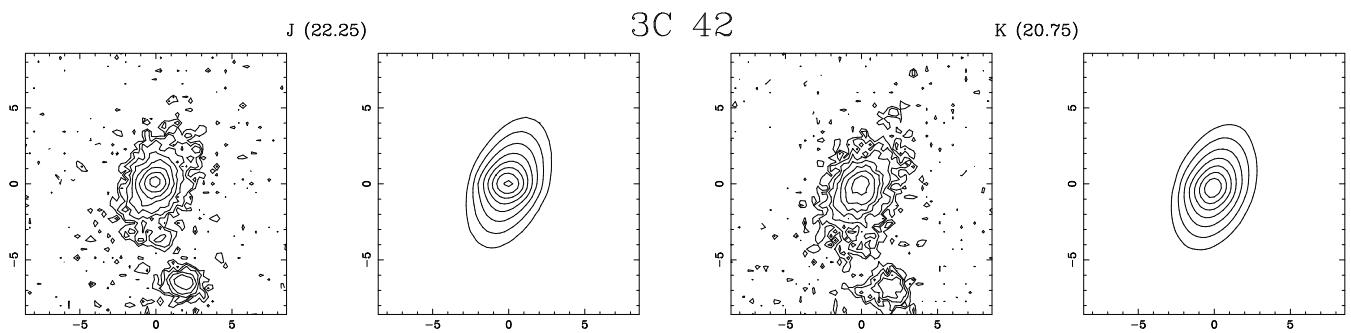


Figure 2. As Fig. 1, but for 3C 42.

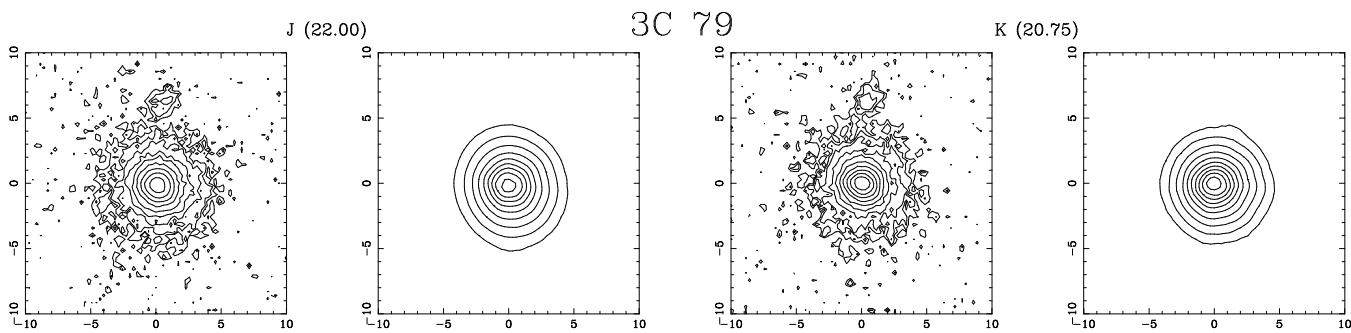


Figure 3. As Fig. 1, but for 3C 79.

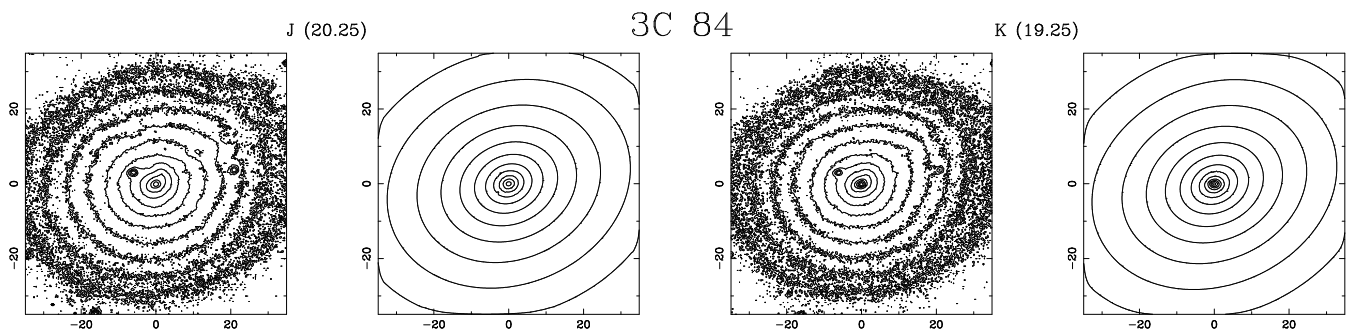


Figure 4. As Fig. 1, but for 3C 84.

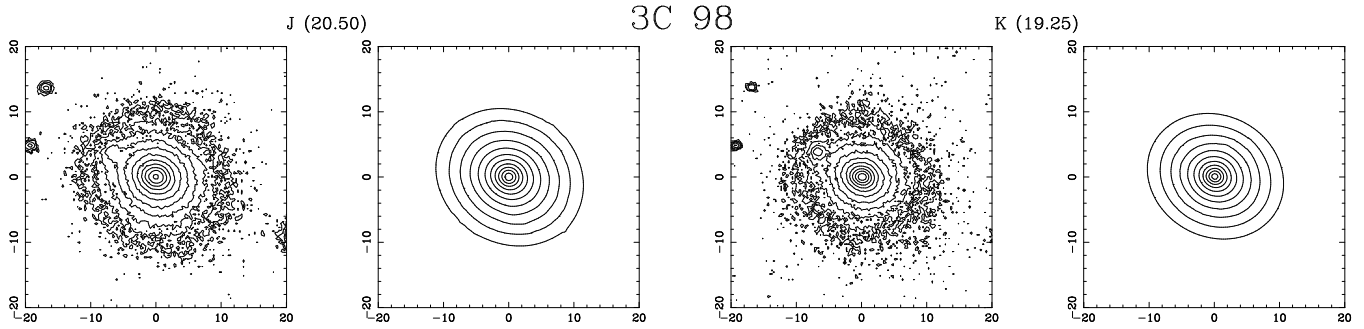


Figure 5. As Fig. 1, but for 3C 98.

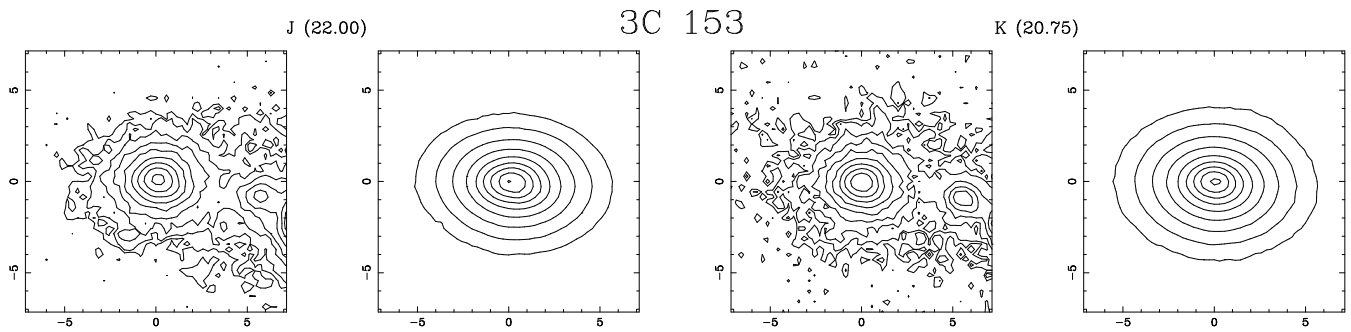


Figure 6. As Fig. 1, but for 3C 153.

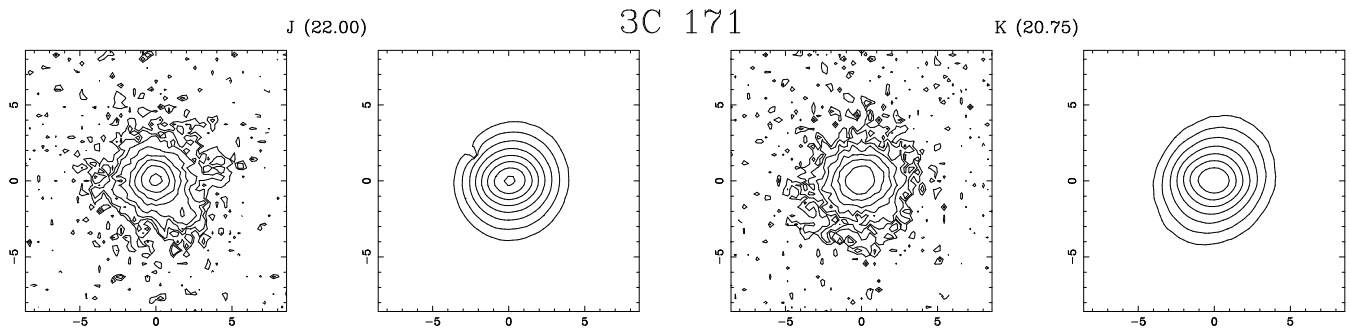


Figure 7. As Fig. 1, but for 3C 171.

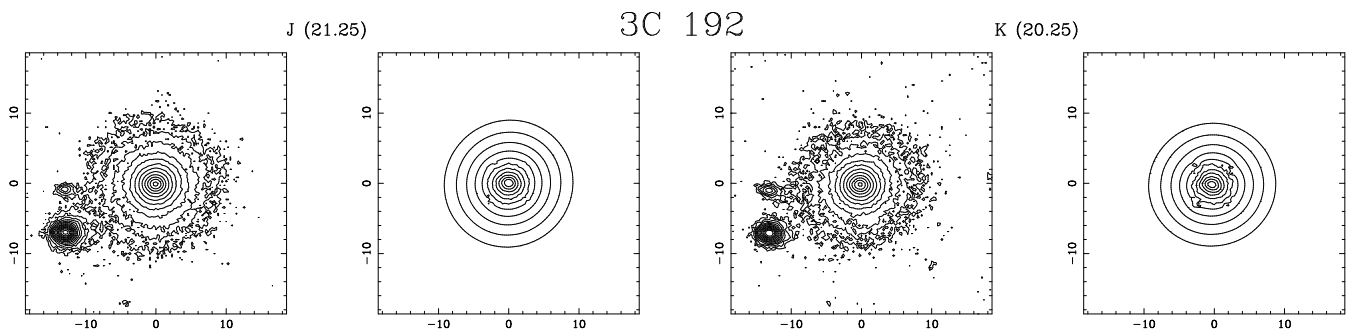
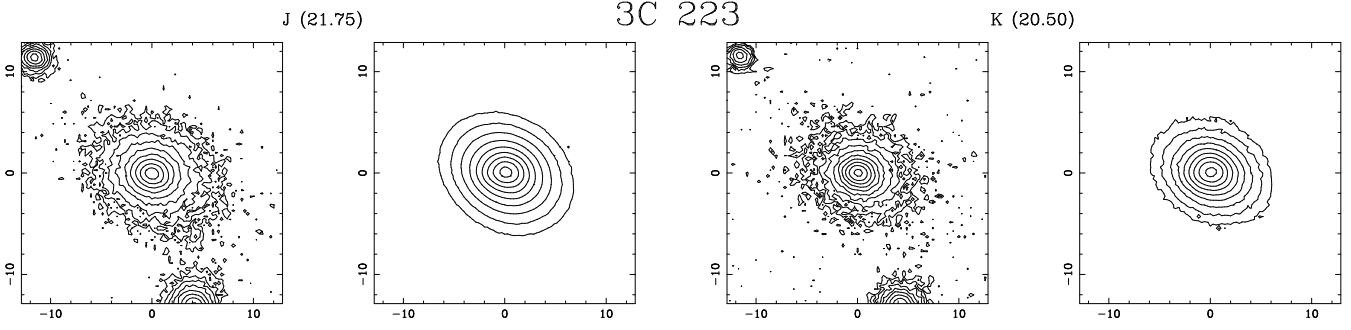
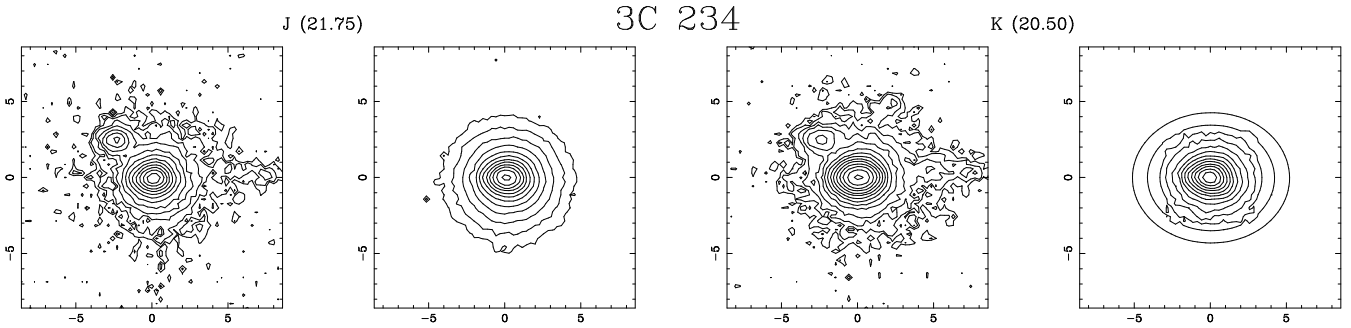


Figure 8. As Fig. 1, but for 3C 192.


Figure 9. As Fig. 1, but for 3C 223.

Figure 10. As Fig. 1, but for 3C 234.

due to a poorly-matched PSF. We shall return to this point in Section 4.2.

3.2 Thermal images

We were able to detect the radio galaxies at L' in eight out of ten cases. We were less successful at M , and only detected three sources of the eight which we observed. For most of our detections, the flux is dominated by the transmitted quasar nucleus, although the stellar contribution is not negligible. The fact that we measure larger fluxes in the larger apertures shows that we have detected starlight from the host galaxies, but the signal-to-noise ratio per pixel is far too low to allow the two-dimensional modelling used for the shorter wavelength images. Indeed, for most galaxies the extended emission is not bright enough to even permit a meaningful measurement of the flux in a circumnuclear annulus. We must therefore estimate the stellar flux by extrapolating from our shorter wavelength images.

The stellar populations of early-type galaxies are dominated in the near-infrared by stars on the red giant branch. We therefore use the observed spectrum of the M2II–III star β Peg (Strecker, Erickson & Witteborn 1979) as a model for the stellar populations of our galaxies. The colours of β Peg are known to match those of early-type galaxies, and the star's spectrum has been used to compute K -corrections for elliptical galaxies (see Longmore & Sharples 1982). We correct the observed 3-arcsec K magnitudes for the presence of the nuclear source listed in Table 3 to determine the flux from stars only in this aperture, and use the β Peg spectrum to estimate the stellar contribution to the flux at L' and M .

Table 4. Inferred magnitudes for the nuclear source in each of the radio galaxies.

Galaxy	J	K	L'	M
3C 33	> 18.20	16.57	12.32	11.33
3C 42	> 19.00	> 18.10	> 15.82	...
3C 79	17.37	15.89	13.11	> 12.54
3C 84	15.70	12.59	9.73	...
3C 98	> 18.50	> 17.20	> 13.10	> 13.46
3C 153	> 18.40	> 17.50	> 16.58	> 12.86
3C 171	> 18.80	> 17.80	> 16.58	> 12.51
3C 192	> 18.40	> 17.40	> 14.99	> 12.63
3C 223	17.52	14.91	12.98	11.81
3C 234	15.54	13.65	10.56	9.94

If there is an excess at greater than 3σ significance in the 3-arcsec aperture, we attribute it to the quasar nucleus. The results of this analysis are presented in Table 4.

Although 3C 98 and 3C 192 are both detected at L' , the emission we observe is purely stellar in origin, as both sources have 3-arcsec aperture $K - L'$ colours consistent with the β Peg spectrum, although the colour of 3C 98 is redder than β Peg's and only marginally consistent with it. However, Lilly et al. (1985a) showed that even in a much larger aperture (7.5 arcsec), 3C 98 is redder than a typical early-type galaxy, which rules out a compact red source as an explanation for the colour. We note that the $L' - M < -0.17$ limit is also consistent with starlight, but is far too blue for a quasar (corresponding to a power law index $\alpha < -2.5$).

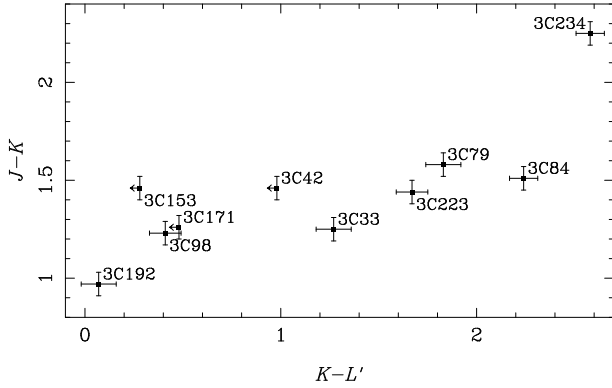


Figure 11. Two colour diagram for the ten radio galaxies. Colours have been measured in a 3-arcsec aperture.

3.3 Reality of our detections

If we examine Fig. 11, which presents the 3-arcsec aperture colours of the ten radio galaxies from Table 2, the galaxies split naturally into two groups: those with $K - L'$ colours consistent with late-type stellar populations, and those which are much redder. There is also a weak, yet highly significant, correlation between the two colours, as expected from a red nuclear component which becomes increasingly significant at K . The simple colour analysis of Section 3.2 will obviously infer a nuclear source for galaxies in the second group only, but it is important to note that these are also the only galaxies for which nuclear sources were detected in Section 3.1. All nuclear sources which are reliably detected at K in our 2D analysis should be detectable in our L' images due to their red colour; this is indeed true. Similarly, any real nuclear sources we detect at J should also be seen at K (and therefore at L' too), and this is also the case. A similar argument does not apply to our M -band data, since the reduction in sensitivity over L' (~ 3 mag) is much greater than can be compensated for by the red colour of the quasar nucleus ($L' - M = 0.76$ for a power law $\alpha = 1.3$; Neugebauer et al. 1987). We are therefore convinced that we have not made any spurious detection, and that we have not failed to detect any sources which are in reality brighter than our quoted limits.

4 LUMINOSITY AND EXTINCTION ESTIMATES

4.1 Galaxies with detected nuclei

If the standard interpretation of our nuclear sources as dust-obscured quasars is correct, they should have the colours of a quasar, modified by some amount of foreground reddening. We therefore perform linear regression, accounting for upper limits in the manner of Isobe, Feigelson & Nelson (1986), on the data of Section 3. This analysis produces values for the intrinsic luminosity and extinction of each nuclear source. We adopt our own parametrization of the near-infrared interstellar extinction law, obtained by fitting a second-order polynomial to the data of Rieke & Lebofsky (1985). This parametrization,

$$A_\lambda/A_V = 0.243\lambda^{-2} + 0.184\lambda^{-1} - 0.022,$$

Table 5. Foreground extinction and unobscured rest-frame $1\ \mu\text{m}$ luminosity for the obscured quasar nuclei detected in our analysis. The dereddened [O III] $\lambda 5007$ emission line luminosity from Table 1 is also listed.

Galaxy	A_V (mag)	$\log L_{1\ \mu\text{m}}$ (W Hz^{-1})	$\log L_{5007}$ (W)
3C 33	29.5 ± 3.5	22.49 ± 0.11	35.23
3C 79	1.0 ± 2.5	23.07 ± 0.25	36.19
3C 84	9.4 ± 1.6	22.02 ± 0.12	35.07
3C 223	3.9 ± 0.6	22.72 ± 0.05	35.53
3C 234	4.0 ± 1.9	23.83 ± 0.15	36.47

by virtue of ignoring the optical data, provides a rather better fit to the longest wavelengths than do those of Howarth (1983) and Cardelli, Clayton & Mathis (1989). The intrinsic quasar spectrum is assumed to be that of an $\alpha = 1.3$ power law (Neugebauer et al. 1987). Table 5 lists the extinctions and intrinsic luminosities we derive for the obscured quasars in the five radio galaxies with detected nuclear sources. These data are presented graphically in Fig. 12. For 3C 223 and 3C 234, where the nucleus was detected at all four wavelengths, we also performed regression with the spectral index as an additional free parameter. In both cases the spectral index was found to be close to 1.3 and the results were not changed significantly.

4.2 Galaxies without detected nuclei

The five galaxies with detected nuclei will obviously preferentially include those objects with low nuclear extinction. If we wish to reach some conclusions about the amount of obscuration in a ‘typical’ radio galaxy, we must make estimates of the extinction in the remaining five members of the sample. This requires us to calculate the intrinsic near-infrared luminosity of the quasars in these objects, which we do in the following manner.

We first estimate the unobscured optical luminosity of the quasar using the [O III] $\lambda 5007$ emission line. Simpson (1998a) has argued that this line is a good indicator of the intrinsic luminosity of radio galaxies and lobe-dominated quasars (such as those selected at low radio frequency). It has also been shown that the [O III] luminosities of lobe- and core-dominated quasars are the same for a given extended radio luminosity (Jackson et al. 1989; Jackson & Browne 1991; Corbin 1997), indicating that the line is emitted isotropically.

There is no Baldwin effect in the equivalent width of [O III] in lobe-dominated quasars (Jackson & Browne 1991). Only when core-dominated objects are considered does such an effect appear. This can be understood as the result of an increase in the continuum luminosity at small polar angles due to an anisotropic component. However, since the near-infrared emission is believed to be produced by dust heated by the optical-ultraviolet radiation and located close to the equatorial plane of the quasar, it is the luminosity at large viewing angles, such as is seen in lobe-dominated quasars, which is of interest to us.

By virtue of the above arguments, we can use the optical-infrared properties of lobe-dominated quasars as benchmarks for the properties of the quasars within our radio galaxies. The mean [O III] equivalent width for the $R < 1$

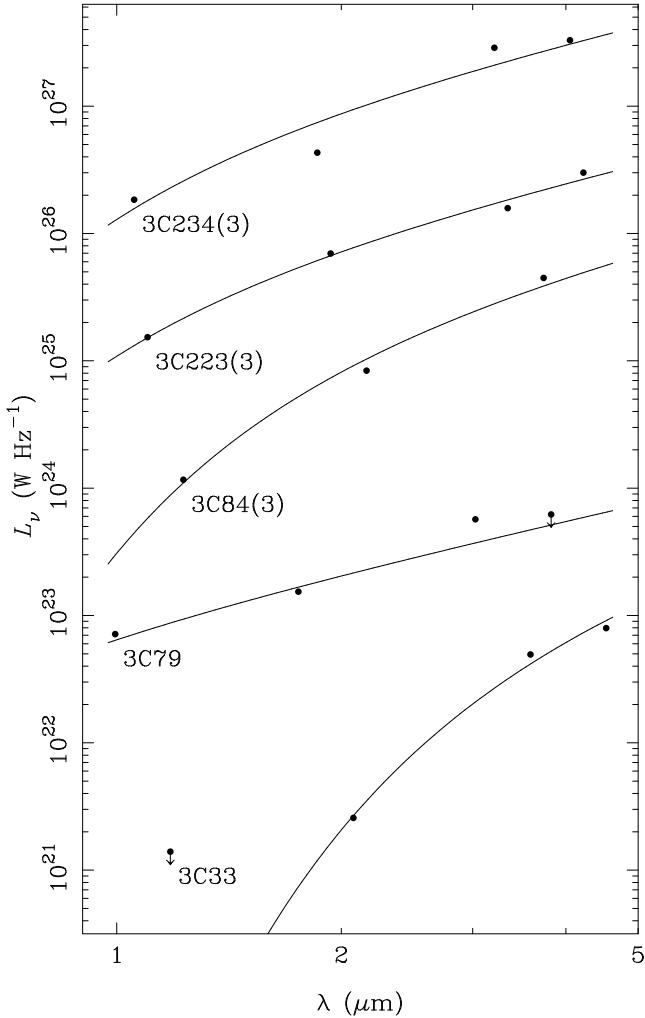


Figure 12. Rest-frame nuclear luminosities and best-fit reddened quasar models for the five radio galaxies in which a nuclear source was detected. For clarity some of the galaxies have been shifted upwards in the y -direction by the number of dex given in parentheses.

quasars from Jackson & Browne (1991) is $\log \text{EW}_{5007} (\text{\AA}) = 1.66 \pm 0.32$, or 46\AA with a factor of 2 scatter. This is larger than the equivalent width of 24\AA determined by Miller et al. (1992) for low redshift ($z < 0.5$) quasars selected from the Palomar–Green Bright Quasar Sample (BQS; Schmidt & Green 1983), because optically selected samples like the BQS preferentially contain objects oriented close to the line of sight where the optical continuum is boosted. This is supported by the large values of the 5-GHz core-to-lobe ratio, R , displayed by the radio-loud quasars in the low redshift BQS (Miller, Rawlings & Saunders 1993).

Adopting 46\AA as the rest-frame equivalent width (with respect to the non-stellar continuum) of the [O III] $\lambda 5007$ emission line, and assuming $\alpha = 0.4 \pm 0.4$ as representative of the continuum between 5007\AA and $1 \mu\text{m}$ (Neugebauer et al. 1987), we find that the last two columns of Table 5 should be related by

$$\log L_{1 \mu\text{m}} - \log L_{5007} = 12.62 \pm 0.34,$$

which is indeed the case, and indicates the validity of our method.

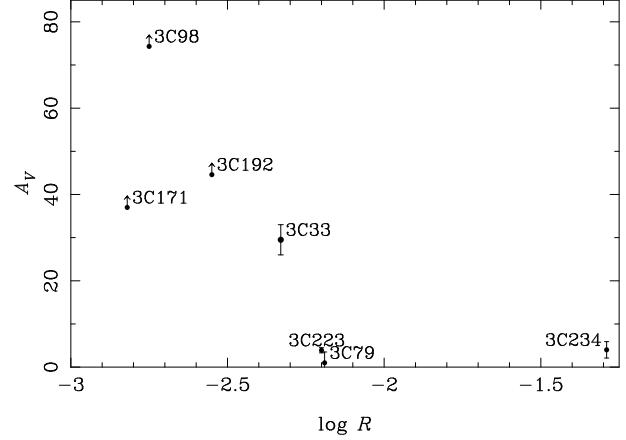


Figure 13. Inferred nuclear extinction for the galaxies in our sample, plotted against the core-to-lobe ratio, R . An anti-correlation is readily apparent.

Applying this technique to the five radio galaxies without detected nuclear sources, we derive lower limits to the nuclear extinction. The non-detections of compact sources in 3C 42 and 3C 153 do not rule out unobscured nuclei with any significance, since both these sources have faint emission line fluxes and therefore are expected to have quite faint nuclei. For the other three galaxies we determine the following 3σ limits: $A_V > 74^m$ for 3C 98; $A_V > 37^m$ for 3C 171; and $A_V > 45^m$ for 3C 192. Note that these limits are derived from the non-detections at M -band (where our sensitivity to highly obscured nuclei is greatest) and are therefore independent of the J and K -band fits. The high extinction towards the nucleus of 3C 98 therefore clearly precludes a K -band nucleus brighter than the limit we quote in Table 3.

5 THE GEOMETRY OF THE OBSCURING MATERIAL

The core dominance parameter, R (also called the core-to-lobe ratio), is a widely-used orientation indicator (Orr & Browne 1982) and we are therefore capable of determining the nuclear extinction to our radio galaxies as a function of viewing angle. Simpson (1994a, 1996) proposed analysing a large sample of radio galaxies in this way to distinguish between different geometries for the obscuring material, which partly provided the motivation for the study described here. The value of R is usually determined at 5 GHz, and the properties of our sources at this frequency are listed in Table A1 of the Appendix. We omit 3C 84 since it does not possess the characteristic FR II radio morphology. The values of the nuclear extinction derived earlier are plotted against $\log R$ in Fig. 13.

Using a generalized Kendall’s rank correlation statistic (Isobe et al. 1986), we can reject the hypothesis that A_V is uncorrelated with R at better than 95% confidence, even if 3C 234 is excluded from the analysis. The nuclear extinction therefore increases with viewing angle (i.e. as R decreases) and suggests a flattened distribution for the obscuring material.

Ignoring density inhomogeneities, the obscuring material’s geometry is defined by $A_V(\theta)$, which we can derive

Table 6. Core dominance parameters and viewing angles with respect to the radio axis for the radio galaxies in our sample.

Galaxy	$\log R$	θ ($^\circ$)
3C 33	-2.33	57^{+16}_{-12}
3C 42	-2.69	64^{+11}_{-13}
3C 79	-2.19	53^{+18}_{-11}
3C 98	-2.75	65^{+12}_{-14}
3C 153	< -3.52	> 54 (2σ)
3C 171	-2.82	67^{+10}_{-15}
3C 192	-2.55	62^{+13}_{-14}
3C 223	-2.20	54^{+17}_{-12}
3C 234	-1.29	33^{+16}_{-7}

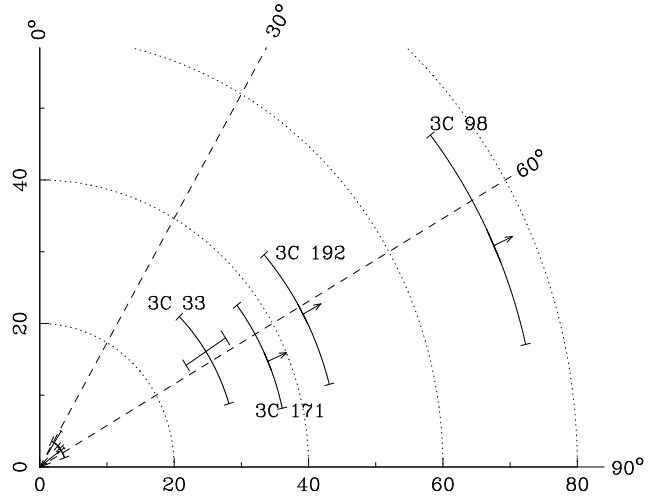
from $A_V(R)$ if we can transform the observed core dominance parameter, R , to a viewing angle, θ . These two quantities are related by

$$R = \frac{1}{2}R_T(1 - \beta \cos \theta)^{-2} + \frac{1}{2}R_T(1 + \beta \cos \theta)^{-2}$$

(Orr & Browne 1982), where $R_T \equiv R(90^\circ)$ and β is the velocity of the beamed core component relative to the speed of light. We adopt $\beta = 0.99$ (Orr & Browne 1982), although its exact value is unimportant except at small values of θ , which are not relevant to our study of radio galaxies.

To convert from R to θ , it is necessary to know the value of R_T . Orr & Browne determined $R_T = 0.024$ from a sample of 3CR quasars, but they assumed that these objects were randomly oriented with respect to the line of sight. Since it is now believed that quasars are preferentially pointed towards us, Orr & Browne's value of R_T will be an overestimate. We therefore redetermine R_T using both quasars and FR II radio galaxies from Laing et al. (1983) with $z < 0.43$, although we exclude 3C 236 since it possesses a steep-spectrum radio core. As described in the Appendix, a good fit to the data is obtained with $P(\log R_T) = N(-2.54, 0.51)$. This is consistent with the distribution derived by Simpson from the radio galaxies alone, and with estimates made from other samples of radio galaxies (e.g. Morganti et al. 1997).

Since we have only determined the *a priori* probability distribution for R_T , and not its actual value for each radio galaxy, the observed core dominance parameter, R , is transformed into a probability distribution for the viewing angle, θ . This transformation is described in the Appendix. We list the viewing angles for the radio galaxies in Table 6 and plot the cross-section through the torus in Fig. 14. It is immediately clear from this analysis that our inability to constrain the angle at which we are viewing each object is a major limitation to the effectiveness of this technique. Doppler boosting only produces a fourfold increase in the observed luminosity of the central component for $\theta \approx 50^\circ$ (the viewing angle which is believed to separate quasars from radio galaxies at low redshift; L94, Simpson 1998a, and see also Table 6), barely enough to produce a signal over the factor of three scatter in R_T . Since core dominance is believed to be the best available orientation indicator, it is clear that a much larger sample of radio galaxies will be needed to produce a useful torus map.

**Figure 14.** A cross section through the torus perpendicular to the equatorial plane. The axes are in units of magnitudes of visual extinction. The dotted lines describe the polar coordinate frame and are there to guide the eye.

6 THE K - Z RELATION AT LOW REDSHIFT

T96 claimed that the K magnitudes of their radio galaxy hosts are 0.5 magnitudes fainter than the currently-assumed K - z relation, with the discrepancy being caused by the contribution from the quasar nucleus. They detected nuclear sources in all twelve of their galaxies, with a mean nuclear-to-host ratio $\langle L_{\text{nuc}}/L_{\text{host}} \rangle = 0.80$. Our study, on the other hand, failed to detect a quasar contribution in five of our objects, despite a similarly faint detection threshold. What effect does our result have on the K - z locus? We find the best least-squares fit to our data that can be obtained by applying an offset, Δ , to the K - z relation of Lilly et al. (1985b),

$$K = 49.87 - \sqrt{1092.7 - 259.74 \log z} + \Delta.$$

For the raw data, the best offset is effectively zero ($\Delta = -0.01$), as expected given the accuracy of our photometry and the unbiased nature of our sample. If we consider instead just the host magnitudes of Table 3, we find $\Delta = 0.10$, supporting a shift of the K - z relation to fainter magnitudes, but by a much smaller amount than that proposed by T96. In addition, this should probably be considered an upper limit to any shift required in the K - z relation, since sources from fainter radio surveys (which lie on same K - z relation due to the lack of a correlation between radio and host galaxy luminosity and low redshift) will have intrinsically fainter infrared nuclei, which should therefore contribute less flux. We display our results in Fig. 15, together with the host galaxy magnitudes derived by T96, which are clearly fainter on average. We investigate this discrepancy, first by addressing the difference in the detection rates for nuclear sources between our study and that of T96, and then by looking at the difference in host galaxy magnitudes. We assume that the nuclear sources we and T96 have detected are in fact active nuclei, based on their luminosities and broad-band SEDs (T96 make a similar claim). If instead they are merely stellar cusps (albeit ones with unusual colours), then there is obviously no reason to shift the K - z relation at all, since

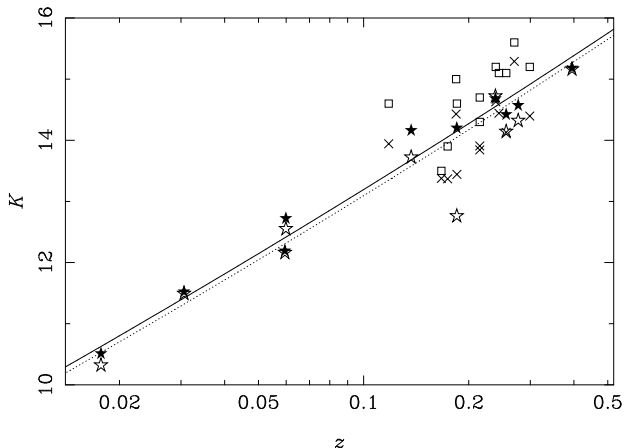


Figure 15. The K -band Hubble diagram for low redshift radio galaxies. Open stars are the observed magnitudes for our 3CRR radio galaxies, filled stars are the model host galaxy magnitudes for these objects, and crosses and open squares are the observed and model host galaxy magnitudes for T96’s radio galaxies (all measured or synthesized in 12-arcsec apertures). The dotted line is the K - z relation from Lilly et al. (1985b), and the solid line is this relation shifted by 0.10 mag to provide the best least-squares fit to our model magnitudes.

the actual form of the radial surface brightness profile is unimportant.

6.1 Detection efficiency

While our sample is effectively complete (only the random exclusion of 3C 123 prevents it from being truly so), the twelve objects studied by T96 were selected to match previously-constructed samples of radio-loud and radio-quiet quasars. One criterion was a match in radio spectral index, and T96’s sample therefore included a number of radio galaxies with spectra much flatter than the typical $\alpha \approx 0.7$. There are five such flat-spectrum radio galaxies in the sample of T96, and they are therefore strongly overrepresented compared to the general low frequency selected radio galaxy population (there are none in our sample). Flat integrated radio spectra are produced when the flat spectrum radio core dominates over the steep spectrum lobes in the frequency region of interest, and consequently such sources have high values of the core-to-lobe parameter, R . Fig. 13 showed the strong anti-correlation between A_V and R , which we interpreted in terms of the geometry of the obscuring material. We should therefore expect the nuclei of T96’s radio galaxies to be less heavily obscured than those of our sample members. This should result in brighter (and hence more readily detectable) nuclei and a tendency for their sources to lie below (i.e. be brighter than) the K - z relation. Indeed, an offset of 0.14 mag to brighter magnitudes needs to be applied to the relation of Lilly et al. (1995b) in order to obtain the best fit to their raw data.

The single-filter imaging of T96 does not permit the detailed method of extinction determination we employed in Section 4.1. Instead we estimate the average extinction for T96’s radio galaxy sample as a whole, by comparing the luminosities of the nuclei detected in the radio galaxies with

those detected in the radio-loud quasars. Due to the way the samples were matched, the intrinsic luminosities of the active nuclei should be the same. Their Tables 4 and 5 indicate that the mean observed luminosity of the radio galaxy nuclei is 1.77 mag fainter than that of the radio-loud quasar nuclei. A similar result is found when the $L_{\text{nuc}}/L_{\text{host}}$ ratios are compared. For a typical redshift $z \approx 0.2$, this corresponds to $A_V \approx 13^m$. By contrast, our sample has an average extinction $A_V > 23^m$.

Our estimate appears to be more in line with the admittedly very limited previous study in this field. Simpson (1994a) studied a small, but complete, sample of nearby radio galaxies from the MS4 survey (Burgess & Hunstead 1994) which included three Class A (Hine & Longair 1979) objects. A nuclear source was detected in one object, which further study revealed to suffer an extinction $A_V = 30 \pm 4^m$ (PKS 0634–205; Simpson et al. 1995). The lower limits determined for the other two Class A sources implied an average $A_V > 21^m$. The powerful radio galaxy Cygnus A has also had its quasar nucleus detected in the near-infrared (Djorgovski et al. 1991), and the most recent extinction estimates indicate very heavy obscuration ($A_V \approx 150^m$; Simpson 1994a, Ward 1996).

We also note that two of T96’s radio galaxies, 3C 219 (L94; Hill et al. 1996) and 3C 287.1 (Erculeous & Halpern 1994) clearly show broad $H\alpha$ in their optical spectra. It is therefore to be expected that these two objects possess bright nuclear sources in the near-infrared. We conclude that T96’s sample is predisposed towards sources with relatively low nuclear obscuration, and believe that our sample, being effectively complete and free from selection biases, is more representative of the radio galaxy population at large.

6.2 Host galaxy magnitudes

Even though T96’s sample of radio galaxies appears to be biased towards objects with low nuclear obscuration, the host galaxies should not be affected. Our multi-wavelength images allow us to compute robust upper limits to the non-stellar flux at K (and hence an upper limit to the shift of the K - z relation required) in a relatively simple manner which does not involve a “black box” routine such as the two-dimensional fitting procedure. First, we assume that all the L' flux in a 3-arcsec aperture arises from the nucleus – since there *must* be some starlight present, this will overestimate the true nuclear flux. In the three instances where no detection was made at L' , we use the 3σ upper limit (again, overestimating the true flux). We then determine an upper limit to the K -band flux by assuming that the spectrum is an unreddened $\alpha = 1.3$ power law. Although there will be variations in the near-infrared spectral indices of the objects in our sample, these should average out among the ten galaxies. We compute the faintest possible host galaxy K -band magnitude by subtracting this nuclear flux from the observed 12-arcsec aperture flux. When this analysis is applied to 3C 234, the maximum nuclear strength we derive exceeds the observed 12-arcsec magnitude, which indicates the conservative nature of our approach. Obviously, we cannot merely exclude 3C 234 from the analysis, since it is the most strongly contaminated source in our sample, so we assume the host has $K = 14.2$, as determined by our model-fitting (T96 obtain a very similar result). Even with these

gross overestimates of the nuclear fluxes (and hence underestimates of the host galaxy brightnesses), the offset from the K - z relation is only $\Delta = 0.35$, somewhat less than the 0.5 mag found by T96. More realistic estimates, such as assuming that the nucleus suffers at least 5 mag of extinction (just enough to obscure broad H α), imply $\Delta < 0.27$. The K - z relation followed by the host galaxies in our sample cannot therefore be the same as that found by T96 for the galaxies in their sample, unless the nuclei of our radio galaxies have intrinsic near-infrared spectral indices of $\alpha < 0.2$. This is obviously incompatible with unification models which claim that the nuclei of radio galaxies are identical to those of quasars.

How then did T96 find such a large shift in the K - z relation? We first rule out the possibility that the galaxies in T96's sample are genuinely fainter than ours. Although T96's sample is generally of lower radio luminosity than ours, Hill & Lilly (1991) have shown that there is no difference in the optical magnitudes of radio galaxies over three orders of magnitude in radio luminosity, and the optical-infrared colours of the two samples cannot differ by half a magnitude. In addition, Eales et al. (1997) have shown that the K magnitudes of radio galaxies from the 3C and 6C samples (6C is selected at a ~ 5 times fainter flux level) are similar at low redshift. Finally, if we exclude those radio galaxies from T96's sample which do not meet the 3CRR flux limit, their result is virtually unchanged. Similarly, if we consider only FR II galaxies from T96, or only those galaxies with a steep radio spectrum, we find no significant change to their result.

We consider two likely explanations for the different K - z relations inferred. We first consider what effect the small field of view ($\sim 35''$) of IRCAM1 might have had on T96's modelling. While the much larger field of view of IRCAM3 provides a significant amount of blank sky in our images and therefore allows an accurate determination of the background level, this was not the case with IRCAM1. As T96 explain, they may have overestimated the sky level in their images, and we discuss here why this can lead to an underestimation of the host galaxy brightness. T96's radio galaxies have a typical effective radius of a few arcseconds. At the edge of their field of view, a de Vaucouleurs profile does not have a negligible surface brightness, but rather will have $\mu \approx 23$ mag arcsec $^{-2}$ (for a typical $\mu_{1/2} \approx 20.5$ and $r_e \approx 6''$). We have investigated the effects of this on modified K -band images of some of our galaxies, by subtracting a constant value from all the pixels to simulate overestimation of the sky level.

We find that for small deviations from the true value, the effective radius of the best-fitting model does not change significantly, but the flux normalization of the stellar component is decreased. This normalization is primarily determined at $r \approx r_e$, since the signal-to-noise ratio is much lower at larger radii, while the sampling errors can be large near the centre, and the flux of the nuclear source can be varied to compensate for deficiencies in the quality of the fit. For a typical galaxy with an error in background determination of the level indicated above, we find an increase of ~ 20 – 40% increase in the flux attributed to the nucleus. The value of the χ^2 statistic also increases, and it is therefore worth considering whether more accurate results might be obtained if

Table 7. Direct comparison between our results and those of the elliptical galaxy fits of Taylor et al. (1996). Host galaxy magnitudes are within a simulated 12-arcsec aperture.

Object		K_{nuc}	K_{host}	$\frac{L_{\text{nuc}}}{L_{\text{host}}}$	r_e	a/b	Θ
3C 79	Us	15.9	14.4	0.35	8.0	1.07	11
	T96	15.2	14.6	0.57	16.6	1.16	7
3C 234	Us	13.6	14.2	1.66	12.2	1.21	81
	T96	14.0	14.3	1.41	13.0	1.22	55

the sky level is included as an extra fitting parameter in the modelling process.

There is also evidence that T96 may have systematically overestimated the scale lengths of their galaxies. Optical imaging with the *Hubble Space Telescope* (Dunlop et al. 2000) produced a median scale length of 12 kpc, compared to 20 kpc determined by T96. The effect of overestimating the r_e is also to lower the contribution from the host galaxy in the central regions, and therefore to overestimate the contribution from a nuclear point source. A systematic error of $\sim +70\%$ in the scale lengths determined by T96 would serve to produce central surface brightnesses ~ 1 mag too faint (again, the fitting procedure will tend to match the model to the data at $r \approx r_e$) and the model flux within a $12''$ aperture will be underestimated by ~ 0.4 – 0.7 mag, depending on the size of the galaxy. Since this is very much in line with the shift determined by T96, it would seem to be a likely explanation for their result.

We can make a direct comparison between our results and those of T96 for the two objects which are common to both samples. We present the results of our K -band fits and those of T96 in Table 7. The agreement for 3C 234 is excellent, but it is less good for 3C 79. Optical imaging with the *Hubble Space Telescope* (Dunlop et al. 2000) produces an effective radius $r_e = 9.4$ kpc, somewhere between the values we determine from our J and K -band images, and clearly indicating that T96 overestimated the true value. A visual inspection of their Fig. A2 appears to indicate that the larger effective radius is influenced by the companion source approximately $6''$ north of the radio galaxy. Alternatively, there may have been additional scattered light within IRCAM1 which would artificially enhance the surface brightness at large radial distances and hence cause the scale length to be incorrectly overdetermined, although the good agreement for 3C 234 (where the bright nuclear point source would be expected to produce a large effect) seems to argue against this explanation.

It is quite possible that different effects are at work for different objects. Since we can think of no likely effect which would serve to *overestimate* the host galaxy brightnesses, we can expect a significant systematic error in the results of T96, even if we cannot be certain what the dominant cause of this error might be.

7 SUMMARY

We have analysed near-infrared $JKL'M$ images of an effectively complete sample of ten 3CRR radio galaxies with strong emission lines, and have separated them into their nuclear and stellar components. We find that the colours of the

nuclear components are well-modelled by a reddened power-law, and the derived unobscured luminosities are in excellent agreement with the values predicted from the emission-line luminosities.

We find evidence that the nuclear extinction increases with viewing angle, suggesting a flattened distribution for the obscuring material. The contributions from the nuclear components make the model host galaxy magnitudes fainter than the observed K magnitudes, and support a shift of the K - z relation to fainter magnitudes by 0.1 mag for low-redshift 3CRR galaxies. Using our observed L' magnitudes and the assumption that the nuclear sources in radio galaxies are intrinsically no bluer than quasar nuclei, we can rule out a shift of more than 0.3 mag, independent of our two-dimensional model-fitting procedure.

We have investigated possible causes of the different results obtained by Taylor et al. (1996) and ourselves. While we believe that T96's sample is biased towards sources with low nuclear obscuration and therefore a relatively large nuclear fraction, this should not affect their host galaxy magnitudes. We believe that their fainter magnitudes are caused by overestimating the sky level in their images and/or the effective radii of their galaxies. We conclude that the magnitudes of low-redshift radio galaxy hosts have been systematically overestimated by no more than about 0.1 mag as a result of non-stellar radiation from the obscured quasar nuclei, and that conclusions drawn so far concerning the cosmic evolution of radio galaxies (e.g. Lilly & Longair 1984; Eales & Rawlings 1996) are therefore reliable.

ACKNOWLEDGMENTS

We are grateful to Jo McAllister for useful discussions regarding the accuracy of the 2-D fitting results, and to the referee, Jim Dunlop, for suggesting improvements to the manuscript. The United Kingdom Infrared Telescope is operated by the Joint Astronomy Centre on behalf of the U. K. Particle Physics and Astronomy Research Council, and we thank the UKIRT staff for their help. We also thank Mike Goad for providing a coded version of the simulated annealing minimization routine. This work has made use of the NASA/IPAC Extragalactic Database (NED), operated by the Jet Propulsion Laboratory, California Institute of Technology, under a contract with the National Aeronautics and Space Administration.

REFERENCES

- Antonucci R. R. J., 1984, *ApJ*, 278, 499
 Baars J. W. M., Genzel R., Pauliny-Toth I. I. K., Witzel A., 1977, *A&A*, 61, 99
 Barthel P. D., 1989, *ApJ*, 336, 606
 Baum S. A., Heckman T., Bridle A., van Breugel W., Miley G., 1988, *ApJS*, 68, 643
 Bridle A. H., Fomalont E. B., 1979, *AJ*, 84, 1679 (BF)
 Burgess A. M., Hunstead R. W., 1994, in Bicknell G. V., Dopita M. A., Quinn P. J., eds, *ASP 54: The First Stromlo Symposium: The Physics of Active Galaxies*. ASP, San Francisco, p. 359
 Burns J. O., Basart J. P., De Young D. S., Ghiglia D. C., 1984, *ApJ*, 283, 515 (BBDG)
 Cardelli J. A., Clayton G. C., Mathis J. S., 1989, *ApJ*, 345, 245
 Corbin M. R., 1997, *ApJS*, 113, 245
 de Vaucouleurs, G., 1948, *Ann. Astrophys.*, 11, 247
 Djorgovski S., Weir N., Matthews K., Graham J. R., 1991, *ApJ*, 372, L67
 Dunlop J. S., McLure R. J., Mukula, M. J., Baum S. A., O'Dea C. P., 2000, *MNRAS*, submitted
 Dunlop J. S., Taylor G. H., Hughes D. H., Robson E. I., 1993, *MNRAS*, 264, 455
 Eales S. A., Rawlings S., 1996, *ApJ*, 460, 68
 Eales S., Rawlings S., Law-Green D., Cotter G., Lacy M., 1997, *MNRAS*, 291, 593
 Eracleous M., Halpern J. P., 1994, *ApJS*, 90, 1
 Fabbiano G., Trinchieri G., Elvis M., Miller L., Longair M., 1984, *ApJ*, 277, 115
 Fanaroff B. L., Riley J. M., 1974, *MNRAS*, 167, 31P
 Fanti R., Fanti C., Schilizzi R. T., Spencer R. E., Rendong N., Parma P., van Breugel W. J. M., Venturi T., 1990, *A&A*, 231, 333 (F90)
 Feigelson E. D., Nelson P. I., 1985, *ApJ*, 293, 192
 Fermini I., Burns J. O., Perley R. A., 1997, *AJ*, 114, 2292 (FBP)
 Fomalont E. B., Bridle A. H., 1978, *AJ*, 83, 725 (FB)
 Giovannini G., Feretti L., Gregorini L., Parma P., 1988, *A&A*, 199, 73 (GFGP)
 Hardcastle M. J., Alexander P., Pooley G. G., Riley J. M., 1998, *MNRAS*, 296, 445 (HAPR)
 Hargrave P. J., McEllin M., 1975, *MNRAS*, 173, 37 (HM)
 Heckman T. M., van Breugel W. J. M., Miley G. K., 1984, *ApJ*, 286, 509 (HvBM)
 Herbig T., Readhead A. C. S., 1992, *ApJS*, 81, 83
 Hill G. J., Lilly S. J., 1991, *ApJ*, 367, 1
 Hill G. J., Goodrich R. W., DePoy, D. L., 1996, *ApJ*, 462, 163
 Hine G., Longair M. S., 1979, *MNRAS*, 188, 111
 Högbom J. A., 1979, *A&AS*, 36, 173 (H79)
 Howarth I. D., 1983, *MNRAS*, 203, 301
 Isobe T., Feigelson E. D., Nelson P. I., 1986, *ApJ*, 306, 490
 Jackson N., Browne I. W. A., 1991, *MNRAS*, 250, 422
 Jackson N., Browne I. W. A., Murphy D. W., Saikia D. J., 1989, *Nature*, 338, 485
 Jenkins C. J., Pooley G. G., Riley J. M., 1977, *MemRAS*, 84, 61 (JPR)
 Laing R. A., 1981, *MNRAS*, 195, 261 (L81)
 Laing R. A., Riley J. M., Longair M. S., 1983, *MNRAS*, 204, 151 (LRL)
 Laing R. A., Jenkins C. R., Wall J. V., Unger S. W., 1994, in Bicknell G. V., Dopita M. A., Quinn P. J., eds, *ASP 54: The First Stromlo Symposium: The Physics of Active Galaxies*. ASP, San Francisco, p. 201 (L94)
 Laing R. A., Wall J. V., Jenkins C. R., Unger S. W., 2000, in preparation
 Latta R. B., 1981, *J. Am. Statistical Association*, 26, 713
 Leahy J. P., Perley R. A., 1991, *AJ*, 102, 537 (LP)
 Lilly S. J., Longair M. S., 1984, *MNRAS*, 211, 833
 Lilly S. J., Longair M. S., Miller L., 1985a, *MNRAS*, 214, 109
 Lilly S. J., Longair M. S., Allington-Smith J. R., 1985b, *MNRAS*, 215, 37
 Longmore A. J., Sharples R. M., 1982, *MNRAS*, 201, 111
 Mack K.-H., Klein U., O'Dea C. P., Willis A. G., 1997, *A&AS*, 123, 423 (MKOW)
 Mayer C. J., 1979, *MNRAS*, 186, 99 (M79)
 Miller P., Rawlings S., Saunders R., Eales S., 1992, *MNRAS*, 254, 93
 Miller P., Rawlings S., Saunders R., 1993, *MNRAS*, 263, 425
 Morganti R., Oosterloo T. A., Reynolds J. E., Tadhunter C. N., Migenes V., 1997, *MNRAS*, 284, 541
 Neugebauer G., Green R. F., Matthews K., Schmidt M., Soifer B. T., Bennett J., 1987, *ApJS*, 63, 615
 Orr M. J. L., Browne I. W. A., 1982, *MNRAS*, 200, 1067
 Pauliny-Toth I. I. K., Kellerman K. I., 1968, *AJ*, 73, 953

- Pooley G. G., Henbest S. N., 1974, *MNRAS*, 169, 477 (PH)
- Press W. H., Teukolsky S. A., Vetterling W. T., Flannery B. P., 1996, *Numerical Recipes in FORTRAN: The Art of Scientific Computing* (Second Edition)
- Rawlings S., Saunders R., 1991, *Nature*, 349, 138
- Rawlings S., Saunders R., Miller P., Jones M. E., Eales S. A., 1990, *MNRAS*, 246, 21P (R90)
- Rawlings S., Lacy M., Sivia D. S., Eales S. A., 1995, *MNRAS*, 274, 428
- Rieke G. H., Lebofsky M. J., 1985, *ApJ*, 288, 618
- Riley J. M., Pooley G. G., 1975, *MemRAS*, 80, 105 (RP)
- Scheuer P. A. G., 1987, in Pearson T. J., Zensus J. A., eds, *Superluminal Radio Sources*. CUP, Cambridge, p. 104
- Schmidt M., Green R. F., 1983, *ApJ*, 269, 352
- Simpson C. J., 1994a, D.Phil. thesis, University of Oxford
- Simpson C., 1994b, *MNRAS*, 271, 247
- Simpson C., 1996, *VA*, 40, 57
- Simpson C., 1998a, *MNRAS*, 297, L39
- Simpson C., 1998b, *A&A*, 338, L47
- Simpson C., Ward M. J., Wilson A. S., 1995, *ApJ*, 454, 683
- Simpson C., Ward M., O'Brien P., Reeves J., 1999, *MNRAS*, 303, L23
- Simpson C., Rawlings S., Lacy M., 1999, *MNRAS*, 306, 828
- Spangler S. R., Myers S. T., Pogge J. J., 1984, *AJ*, 89, 1478 (SMP)
- Strecker D. W., Erickson E. F., Witteborn F. C., 1979, *ApJS*, 41, 501
- Taylor G. L., Dunlop J. S., Hughes D. H., Robson E. I., 1996, *MNRAS*, 283, 930 (T96)
- van Breugel W., Jagers W., 1982, *A&AS*, 49, 529 (vBJ)
- van Breugel W., Miley G., Heckman T., 1984, *AJ*, 89, 5 (vBMH)
- Ward M. J., 1996, in Harris D. E., Carilli C. L., eds, *Cygnus A: Study of a Radio Galaxy*. CUP, Cambridge, p. 43
- Yee H. K. C., Oke J. B., 1978, *ApJ*, 226, 753
- Young S., Axon D. J., Hough J. H., Fabian A. C., Ward M. J., 1998, *MNRAS*, 294, 478
- Young S., Hough J. H., Efstathiou A., Wills B. J., Axon D. J., Bailey J. A., Ward M. J., 1996, *MNRAS*, 279, L72

APPENDIX A: CORE DOMINANCE AND VIEWING ANGLE

This Appendix describes how we have used the observed core dominance parameter of a radio galaxy to infer the viewing angle between its radio axis and our line of sight. To do this, we have compiled in Table A1 radio data for all FR II sources with $z < 0.43$ in Laing et al. (1983). In the interests of keeping a homogeneous dataset, we use the 5-GHz flux measurements and spectral indices between 2.7 and 5 GHz from Pauliny-Toth & Kellerman (1968). Although these are not necessarily the most accurate data available, this is not a concern as our assumption of a common spectral index $\alpha = 0$ for the core components (which may be somewhat variable) will introduce some errors in our determination of the rest-frame 5-GHz core dominance parameter. For the four non-3C sources which were not observed by Pauliny-Toth & Kellerman, we have opted to use the data from Herbig & Readhead (1992). These authors perform fits to the radio spectra of sources, which should also help to homogenize the data they compile from the literature. Herbig & Readhead list luminosities and spectral indices at a rest-frame frequency of 2.5 GHz, which we use to compute a rest-frame 5-GHz flux. However, for consistency in Table A1, we list synthetic *observed-frame* 5-GHz fluxes determined from their fits. Note that although we have included

Hine & Longair (1979) Class B radio galaxies in this sample to improve the statistics (the published spectroscopy of the late-RA sources is too poor to make completely accurate classifications and we would therefore have to exclude all of them), their R distribution is not significantly different from that of the Class A objects (a result also found by Morganti et al. 1997).

The first step in our procedure is to determine the distribution of the transverse core dominance parameter, R_T . We construct synthetic samples of 5000 radio sources which are randomly oriented with respect to the line of sight, and have the logarithms of their transverse core dominance parameters, $\log R_T$, drawn from a Normal distribution, whose mean and standard deviation we vary to determine the best fit to the observed data. We quantify the goodness-of-fit using the Peto-Prentice generalized Wilcoxon test (Latta 1981; Feigelson & Nelson 1985), as employed in the ASURV package within IRAF/STSDAS. Of the various tests Feigelson & Nelson list to compare two samples of censored data, this is believed to be the least affected by differences in sample size and censoring patterns, which is important here since our synthetic sample is much larger than the real dataset and suffers no censoring. The best fit we find is when the transverse core dominance parameter is drawn from the distribution $N(-2.54, 0.51)$, with the probability that the two distributions are drawn from the same population being 99.9%. Both versions of the Gehan test (also available in ASURV) produce the same result, so it is not sensitive to the specific test used. Note that the underlying distribution, $\log R_T \in N(-2.43, 0.50)$, reported by Simpson (1998b) was computed using a few older core flux measurements (generally upper limits which have been superseded by more sensitive limits or faint detections), and with a different goodness-of-fit statistic. However, there is only a slight difference between the two distributions, which does not affect the results in that paper.

Having derived a distribution function for $\log R_T$, it becomes possible to infer the probability distribution of viewing angles, $P(\theta|R)$. Bayes' Theorem informs us that

$$P(\theta|R) \propto P(R|\theta)P(\theta).$$

Since R and θ are directly related by R_T , we can write the first term on the right hand side as an *a priori* probability that R_T lies in the appropriate range to produce the observed value of R given that the viewing angle lies in the interval between θ and $\theta + \delta\theta$. If we define $x \equiv \beta \cos \theta$, it is trivial to show that $R/R_T = (1 + x^2)(1 - x^2)^{-2}$. Hence,

$$P(R|\theta) = P(\log R_T = \log R \frac{(1 - x^2)^2}{1 + x^2}) \frac{d \log R_T}{d\theta},$$

and, straightforwardly,

$$\frac{d(\log R_T)}{d\theta} = \frac{\beta \sin \theta}{\ln 10} \frac{2x(3 + x^2)}{1 - x^4}.$$

Finally, we need to consider the *a priori* distribution of viewing angles, $P(\theta)$. A natural choice, motivated by the radio galaxy-quasar unification scenarios, would be to assume that $P(\theta) \propto \sin \theta$ for angles greater than some critical angle, θ_c , and zero for angles less than this. In practice, the actual choice of θ_c has little effect on the results, except for sources with bright radio cores, such as 3C 234, when the probability distribution of angles piles up at the critical

Table A1. Properties of 3CRR FR II radio sources with $z < 0.43$. The total 5-GHz fluxes and spectral indices between 2.7 and 5 GHz are from Pauliny-Toth & Kellerman (1968) except where an asterisk (*) denotes synthesized data from the spectral fits of Herbig & Readhead (1992). We preferentially use 5-GHz core flux measurements, where available, and assume a flat spectrum to convert measurements at other frequencies. The last column identifies which paper in the reference list was used to determine the core flux. Fluxes cited as from LP (Leahy & Perley 1991) are estimated from their radio maps.

Name	z	$S_{5\text{GHz}}^{\text{tot}}$ (Jy)	$\alpha_{2.7}^5$	S^{core} (mJy)	$\log R$	Core ref
3C 16	0.4050	0.51	0.99	< 0.5	< -3.15	LP
3C 20	0.1740	4.18	0.70	2.6	-3.25	FBP
3C 33	0.0595	5.03	0.57	24.0	-2.33	HM
3C 33.1	0.1810	0.86	1.13	15.0	-1.83	vBJ
3C 35	0.0670	0.59	1.31	14.0	-1.65	vBJ
3C 42	0.3950	0.84	1.03	2.4	-2.69	FBP
3C 47	0.4250	1.10	1.01	80.0	-1.27	PH
3C 61.1	0.1860	1.91	1.08	2.3	-3.00	GFGP
3C 67	0.3012	0.91	0.99	337.0	-0.40	vBMH
3C 79	0.2559	1.31	1.01	10.5	-2.19	SMP
3C 98	0.0306	4.97	0.96	9.0	-2.75	FB
3C 109	0.3056	1.64	0.64	320.0	-0.71	RP
4C 14.11*	0.2070	0.89	0.73	29.7	-1.52	HAPR
3C 123	0.2177	16.32	0.83	108.9	-2.24	HAPR
3C 132	0.2140	1.05	1.00	4.1	-2.49	HAPR
3C 153	0.2769	1.35	0.87	< 0.5	< -3.52	HAPR
3C 171	0.2384	1.22	0.80	2.2	-2.82	GFGP
3C 173.1	0.2920	0.77	1.01	7.4	-2.13	GFGP
3C 184.1	0.1182	1.24	0.73	6.0	-2.35	RP
DA 240*	0.0350	0.69	0.95	121.9	-0.69	MKOW
3C 192	0.0598	2.05	0.71	6.0	-2.55	H79
4C 14.27*	0.3920	0.39	0.99	< 0.5	< -3.03	LP
3C 215	0.4110	0.41	0.85	20.0	-1.42	PH
3C 219	0.1744	2.29	1.04	51.6	-1.71	HAPR
3C 223	0.1368	1.29	0.75	9.0	-2.20	RP
4C 73.08*	0.0581	0.90	0.84	19.0	-1.69	M79
3C 234	0.1848	1.54	1.04	90.0	-1.29	RP
3C 244.1	0.4280	1.12	0.89	< 0.6	< -3.41	GFGP
3C 249.1	0.3110	0.78	0.94	110.0	-0.91	PH
3C 268.3	0.3710	1.09	0.96	< 20.0	< -1.86	F90
3C 274.1	0.4220	0.76	1.08	< 6.0	< -2.27	JPR
3C 284	0.2394	0.69	0.71	3.2	-2.40	GFGP
3C 285	0.0794	0.76	0.81	6.8	-2.07	HAPR
3C 300	0.2700	1.10	0.90	9.0	-2.18	RP
3C 303	0.1410	0.94	0.80	150.0	-0.78	PH
3C 319	0.1920	0.65	1.07	< 1.0	< -2.89	BF
3C 321	0.0960	1.22	0.83	30.0	-1.63	JPR
3C 326	0.0895	0.48	1.63	3.5	-2.20	R90
3C 349	0.2050	1.14	0.80	24.0	-1.73	JPR
3C 351	0.3710	1.21	0.84	15.0	-2.02	L81
3C 381	0.1605	1.29	0.94	5.2	-2.45	F84
3C 382	0.0578	2.22	0.74	251.2	-0.91	HAPR
3C 388	0.0908	1.77	0.91	57.9	-1.51	HAPR
3C 390.3	0.0569	4.48	0.62	340.0	-1.10	vBJ
3C 401	0.2010	1.37	1.14	32.0	-1.71	BBDG
3C 436	0.2145	0.99	0.99	20.0	-1.77	RP
3C 438	0.2900	1.54	1.20	10.0	-2.32	L81
3C 452	0.0811	3.26	0.95	130.0	-1.42	RP
3C 457	0.4270	0.55	0.93	6.0	-2.10	LRL

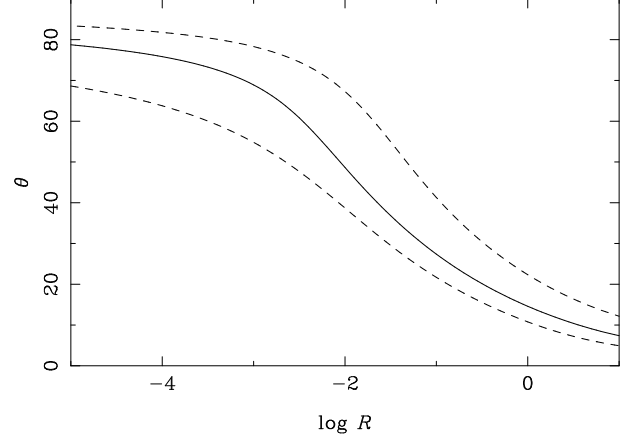


Figure A1. The *a posteriori* probability density function of viewing angle, θ , as a function of core-to-lobe ratio, R , under the assumption described in the text. The solid line indicates the maximum of the pdf, and the dashed lines show the 1σ limits.

angle. Rather than adopt an *ad hoc* formulation to create a smooth transition at $\theta \approx \theta_c$ and prevent this unrealistic behaviour, we choose $\theta_c = 0$. The behaviour of $\theta(R)$ under these assumptions is shown graphically in Fig. A1.